AGU PUBLICATIONS

JGR

Journal of Geophysical Research: Space Physics

RESEARCH ARTICLE

10.1002/2015JA021444

An empirical profile of VLF triggered emissions

J. D. Li[1], M. Spasojevic[1], and U. S. Inan[1,2]

[1]Department of Electrical Engineering, Stanford University, Stanford, California, USA, [2]Department of Electrical Engineering, Koc University, Istanbul, Turkey

Key Points:
- Risers undergo a larger net frequency change and can endure for a longer duration than fallers
- Triggering behavior at initiation depends on the transmitted element but later becomes independent
- The number of triggered emissions correlates with the total transmitted signal growth and with *Kp*

Correspondence to:
J. D. Li,
jdli@stanford.edu

Citation:
Li, J. D., M. Spasojevic, and U. S. Inan (2015), An empirical profile of VLF triggered emissions, *J. Geophys. Res. Space Physics*, *120*, 6581–6595, doi:10.1002/2015JA021444.

Received 11 MAY 2015
Accepted 5 AUG 2015
Accepted article online 10 AUG 2015
Published online 28 AUG 2015

Abstract The Siple Transmitter Experiment operated from 1973 to 1988 and generated a wealth of observations of nonlinear wave-particle interactions including extensive recordings of triggered emissions generated by VLF signals injected into the magnetosphere from the transmitter at Siple Station, Antarctica. Due to their complex appearance and immensely varied behavior, triggered emissions remain poorly described and understood. This work provides a comprehensive statistical description of observed triggered emissions and establishes statistical bounds on triggered emission type (fallers, risers, and positive and negative hooks) and behavior (frequency changes between 1 kHz and 2.5 kHz with initial sweep rates between −2.5 kHz/s and 2.5 kHz/s, with risers undergoing a median frequency change of 556 Hz and fallers a median frequency change of −198 Hz). The statistical study also reveals an apparent dependence of the triggered emission behavior on the transmitted signal itself. Long tones and rising ramps generate more risers and positive hooks, while short tones and falling ramps produce more fallers and negative hooks. Triggered emissions also appear to favorably initiate with sweep rates similar to that of the triggering element, with the 1 kHz/s rising ramps triggering initial risers with a median sweep rate of 1.03 kHz/s and −1 kHz/s triggering initial fallers with a median sweep rate of −0.73 kHz/s. These results improve observations of wave modification resulting from wave-particle interactions in the radiation belts and can be used to validate numerical simulations of triggered emissions.

1. Introduction

Early observations of free-running plasma emissions in the magnetosphere triggered from terrestrial radio signals in the extremely low frequency and very low frequency (ELF/VLF, 0.3–30 kHz) prompted interest in understanding the physics of the wave-particle interactions governing this behavior [*Helliwell et al.*, 1964; *Helliwell*, 1970]. The detection of triggering from VLF Morse code broadcasts by Navy transmitters in the 20–30 kHz band led to interest in establishing dedicated transmission facilities to conduct more controlled experiments [*Helliwell et al.*, 1964]. The most ambitious and prolific experiment so far is the Siple Station experiment in Antarctica, which operated from 1973 to 1988. Experiments utilizing the Siple transmitter produced numerous observations of magnetospheric wave-particle interactions resulting in the generation of free-running plasma emissions triggered from the injected transmissions [*Helliwell*, 1970, 1979, 1988a], and data from the Siple transmitter remain the preeminent source for validating computer simulations of whistler mode wave-particle interactions [*Gibby et al.*, 2008; *Hikishima and Omura*, 2012; *Nunn et al.*, 2003].

In these experiments, ELF/VLF waves radiated by the transmitter at Siple Station propagated into the magnetosphere where they interacted with energetic electrons. The interactions modified the waves, amplifying them and generating new emissions with varying frequency components, known as triggered emissions. The modified waves were then observed by radio receivers on the ground at the Northern Hemisphere conjugate point. The transmitter at Siple Station, Antarctica, (75.93°S, 84.25°W geographic and $L = 4.2$) could transmit frequencies between 1 and 5 kHz, and, for the data used here, a receiving station in the conjugate hemisphere at Lake Mistissini, Canada, (50.42°N, 73.87°W geographic) recorded the received signals. The Antarctic location provides 2–3 km of dielectric isolation from the conducting ground, reducing near-field image currents, and its latitude corresponds to a magnetospheric interaction region with abundant natural VLF activity [*Helliwell and Crystal*, 1973]. As the data were recorded on magnetic tape, a major effort has been undertaken in recent years to restore and archive data collected in the Siple Station experiment [*Li et al.*, 2014] for analysis with modern computing resources and analytic techniques.

Here we analyze a database of receptions of a minidiagnostic (MDIAG) format transmitted by Siple in 1986, which included long and short fixed frequency tones, falling frequency ramps, and a pair of tones closely spaced in frequency, under a variety of times and conditions in order to build a statistical understanding of the time-frequency behavior of triggered emissions (TEs). We also apply the same analytic process to study triggering from the staircase coherence (STACO) format, which includes rising and falling frequency ramps, to further extend our analysis of the effect of the triggering signal on triggered emissions. Past experimental work solely focused on triggering from fixed frequency tones, but here, by considering observations of triggered emissions based on the different triggering elements, we show that the triggering element has a significant effect on the resulting triggered emission. By quantifying the overall frequency change, we then show that the physical process governing the free-running behavior of triggered emissions is effectively independent of the triggering signal once the triggered emission begins. These statistical bounds on the properties of the behavior of triggered emissions are important for evaluating our theoretical understanding of the triggered emission generation mechanism and the validity of numerical simulations.

2. Past Observations and Modeling Efforts

To frame this statistical understanding of triggered emission behavior and to provide some background to understanding triggered emissions, we include a brief review of related past research. Similarly, in order to interpret the experimental results, we have also included a short review of the three common numerical models used to simulate triggered emissions and provide theoretical interpretation.

The generation of free-running emissions is a key feature of the coherent wave instability. Triggered emissions typically occur after the transmitted signal undergoes a period of exponential temporal growth and generally take the form of narrowband rising, falling, or various hook-like elements. These basic forms are commonly referred to as risers, fallers, and hooks [*Helliwell and Carpenter*, 1962; *Helliwell*, 1965]. The earliest work observed the generation of these triggered emissions from Morse code VLF Navy transmissions [*Helliwell et al.*, 1964; *Helliwell*, 1965; *Kimura*, 1968; *Lasch*, 1969] or from natural signals such as whistlers [*Carpenter et al.*, 1969], while later work focused on observations of triggered emissions from Siple transmissions [*Helliwell and Katsufrakis*, 1974; *Stiles and Helliwell*, 1977; *Helliwell*, 1988a, 1988b; *Sa*, 1990]. Repeated observations of triggered emission behavior provided phenomenological descriptions of conditions for triggering. *Stiles and Helliwell* [1975] found that triggering occurs only after the transmitted pulses undergoes its exponential growth and saturates, and *Helliwell* [1988b] observed that triggering usually generates risers and can occur repeatedly until the transmitted pulse ends. The falling triggered emissions, fallers, were observed to occur when the signal terminates near the saturation level and when the transmitted pulses were short in duration, $<$200 ms [*Lasch*, 1969; *Helliwell and Katsufrakis*, 1974]. The saturation level is the amplitude at which the nonlinear amplification of the injected frequency signal terminates and after which other nonlinear effects, such as triggered emissions, may occur [*Gibby et al.*, 2008]. Rising and falling triggered emissions, and the times at which the triggering begins, were also found to relate to phase advances in the transmitted pulse [*Paschal*, 1988, chap. 4].

Numerical modeling of triggered emissions has proven to be an incredibly challenging task. While various numerical approaches have provided insight into the triggering process and behavior, modeling attempts have not successfully reproduced the entire range of triggered emission behavior. Both hybrid [*Katoh and Omura*, 2006] and full [*Hikishima et al.*, 2010] particle-in-cell (PIC) codes successfully simulated rising tone triggered emissions, and the results suggest that triggering occurs at the back end of the input signal near the magnetic equator and that the resonant current formation by untrapped electrons plays an important role in the triggering process. Using the Vlasov Hybrid Simulation (VHS) code, *Nunn et al.* [2005] performed a parametric study and found that low-input amplitudes generate fallers, intermediate-input amplitudes generate risers, and large-input amplitudes generate fallers or hooks. The frequency sweep rate of the resulting triggered emission was shown to be most dependent on the cold plasma density, where lower densities resulted in higher sweep rates. Phenomenological approaches [*Helliwell*, 1967; *Trakhtengerts et al.*, 2003] have proven to be very general in generating any desired form of triggered emission, with the spectral form of the triggered emission primarily dependent on the position and motion of the locus of the interaction region. However, these approaches are otherwise difficult to evaluate due to the large number of free parameters.

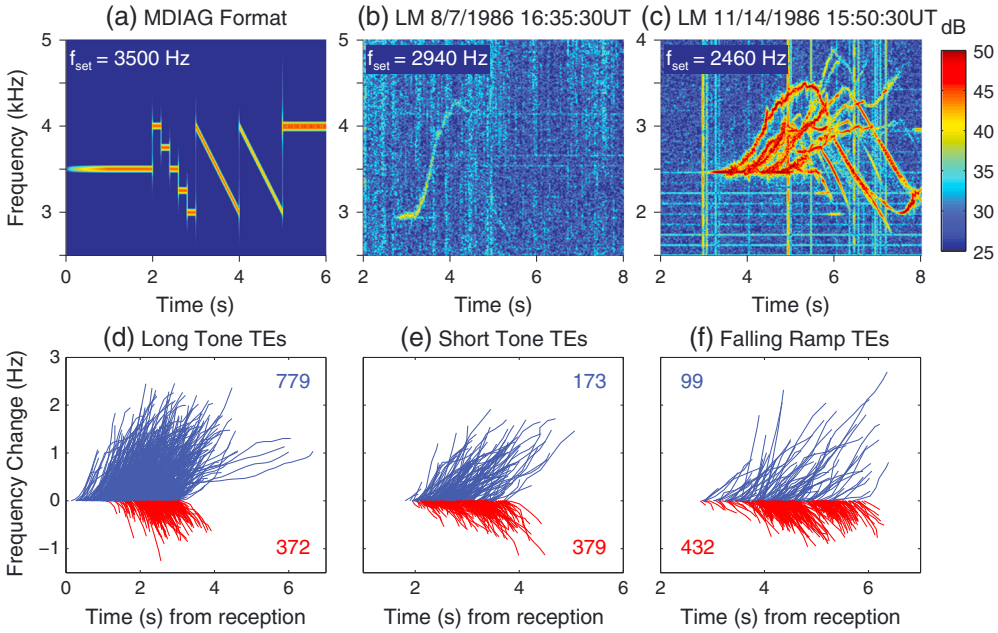

Figure 1. Spectrograms of (a) the transmitted MDIAG format and two conjugate hemisphere receptions with (b) a canonical simple riser and (c) a wide variety of triggered emissions. All collected triggered emissions are overlaid on the same plot to show the frequency and time profiles of risers (blue) and fallers (red) triggered from the transmitted (d) long tone, (e) short tones, and (f) falling ramps. The vertical axis describes the triggered emission's frequency change relative to its initial triggering frequency, and the horizontal axis describes the triggered emission's initiation time relative to the time at which the transmitted signal was received. The triggered emissions from the doublets are not included in the spectrogram or as an overlay plot due to an insufficient number of observations. For clarity in displaying the overlay plots, hooks are not included as they would overlap with and obscure the risers and fallers, and the color-coded numbers in Figures 1d–1f describe the number of plotted risers (blue) and fallers (red) for each triggering element.

3. The 1986 MDIAG and STACO Data Set

We characterize triggered emission behavior by examining two transmission formats and their associated triggered emissions that were received at the Lake Mistissini receiver during 1986. The first format is the minidiagnostic format, abbreviated MDIAG, which was commonly transmitted by Siple Station in 1986 and is shown in spectrogram format in Figure 1a. The entire transmission is centered on an operator-selected tuning frequency, f_{set}, which ranged from 1680 Hz to 5100 Hz. The format is composed of a 2 s "long" tone at f_{set}, five 200 ms "short" tones, two 1 s −1 kHz/s "falling ramps" centered at f_{set}, and a 7 s dual-frequency tone, "doublet," spaced 30 Hz apart and centered on f_{set}+495 Hz. The long tone begins with a power ramp, where the transmitted power is increased from −10 dB to 0 dB over the first second. The short tones descend in a staircase from +500 Hz to −500 Hz from f_{set} in 250 Hz steps. The second of the two frequency ramps is transmitted at −6 dB below the power of the first ramp. Data from the conjugate receiving station in Lake Mistissini, Canada, are available for 1143 transmissions of the MDIAG format, and 444 receptions were detected for a 39% reception rate. The format was originally used for assessing reception conditions to determine if other studies could be conducted, and similar diagnostic transmission formats were used throughout the operation of Siple Station.

Two case examples of MDIAG receptions are shown in Figures 1b and 1c and highlight the wide range of triggered emission behavior. Figure 1b illustrates a canonical riser, which initiates from the long tone and then rises in frequency at a relatively constant frequency sweep rate. In contrast, Figure 1c demonstrates the more common behavior, where a number of triggered emissions are triggered by the injected signal. Here we see that not only are risers excited, but fallers and hooks (triggered emissions that change from a riser to a faller or vice versa) are also generated. To develop our data set of 3469 triggered emissions excited from our 444 MDIAG transmissions, we first processed each transmission to generate a high time and frequency resolution spectrogram. Using the spectrogram, we considered narrower time and frequency windows around each type of triggering element (long tone, short tones, ramps, and doublet) and manually identified and selected time and frequency points corresponding to each triggered emission. Each triggered emission

Table 1. Table of MDIAG and STACO Triggered Emission Statistics in 1986, Illustrating the Overall Number of Triggered Emissions, Divided Into Risers, Fallers, and Hooks, With Hooks Further Subdivided Into Positive (Initially Rising) and Negative (Initially Falling) Hooks[a]

	Risers		Fallers		Hooks		Positive		Negative	
	Count	%	Count	%	Count	%	Count	%	Count	%
MDIAG										
All	1111	32%	1220	35%	1138	33%	759	22%	379	11%
Long tone	779	45%	372	21%	585	34%	505	29%	80	4.6%
Short tones	173	22%	379	49%	227	29%	124	16%	103	13%
Falling ramps	99	13%	432	56%	246	32%	65	8.4%	181	23%
Doublet	43	39%	15	14%	51	47%	44	40%	7	6.4%
STACO										
All	474	40%	225	19%	484	41%	409	35%	75	6.3%
Rising ramps	458	51%	27	3.0%	405	46%	404	45%	1	0.1%
Falling ramps	14	4.8%	198	68%	79	27%	5	1.7%	74	25%

[a]The percentage describes the percentage of each type of triggered emission excited by a given transmission element. The percentages for risers, fallers, and hooks sum to 100%, while the positive and negative hook percentages sum to the percentage of hooks. The top half describes the overall results for the MDIAG format and subdivided into the long tone, short tones, falling ramps, and doublet elements, while the lower half describes the overall results for the STACO format with subdivisions for the rising and falling ramps.

was then labeled based on its frequency behavior, where signals that only increased or decreased in frequency were labeled as risers or fallers and signals that both increased and decreased in frequency were labeled as hooks. The results are compiled in Table 1. Hooks are also further subdivided into positive hooks, hooks that initially rise in frequency, and negative hooks, hooks that initially fall in frequency. The upper half of Table 1 categorizes the number and percentage of triggered emissions triggered by each transmission element (long tone, short tones, falling ramps, and doublet) of the MDIAG format.

To characterize an aggregate profile of all 3469 triggered emissions, overlay plots in Figures 1d–1f plot the aggregate time-frequency profile of risers (blue) and fallers (red) differentiated by the triggering element. For clarity, the hooks are not shown on these plots due to their overlap with other triggered emissions. The vertical axis describes the frequency change of the triggered emissions relative to their initial initiation frequency, while the horizontal axis describes when the triggered emissions began relative to when the triggering MDIAG transmission was received. The triggering transmission element plays a significant role in the determining the resulting type of triggered emission, but, in general, risers initiate earlier than fallers and extend to higher frequencies and endure for longer durations. The triggered emissions triggered from doublets are not shown, as they account for only 109 triggered emissions. Doublets exhibit a suppression effect [*Helliwell et al.*, 1986] that suppresses the amplification of the doublet signals and disturbs the conditions conducive for generating triggered emissions.

As the MDIAG format only includes falling frequency ramps, we also examine the behavior of triggered emissions from a second transmission format called the staircase coherence format, abbreviated STACO, which includes both rising and falling frequency ramps. The STACO format, transmitted by Siple from July to December of 1986, is illustrated in Figure 2a and is composed of two identical sets of rising, 1 kHz/s ramp elements (Riser 1 and Riser 2), followed by two identical sets of falling, −1 kHz/s ramp elements (Faller 1 and Faller 2). Each ramp set contains five 1 s elements approximating an ideal frequency ramp composed of 1 ms, 10 ms, 25 ms, 50 ms, and 100 ms long tones. The entire transmission is centered on an operator-selected tuning frequency, f_{set}, which ranged from 1680 Hz to 4020 Hz. Data from the conjugate receiving station are available for 170 transmissions of the STACO format, and 63 receptions were detected for a 37% reception rate, although one case is excluded from further analysis due an operator transmission error. The format was originally intended for studying the required time-frequency spacing to approximate a continuous frequency ramp [*Mielke and Helliwell*, 1993] and has also been recently used to quantify the observed preferential nonlinear amplification of rising ramps over falling ramps [*Li et al.*, 2015].

An example of a STACO reception is shown in Figure 2b, with the white lines at 3980 Hz and 2980 Hz marking the frequency extent of the transmitted signals in order to highlight the triggered emissions rising and falling at the end of the ramp elements. To characterize an aggregate profile of the 1183 triggered emissions excited

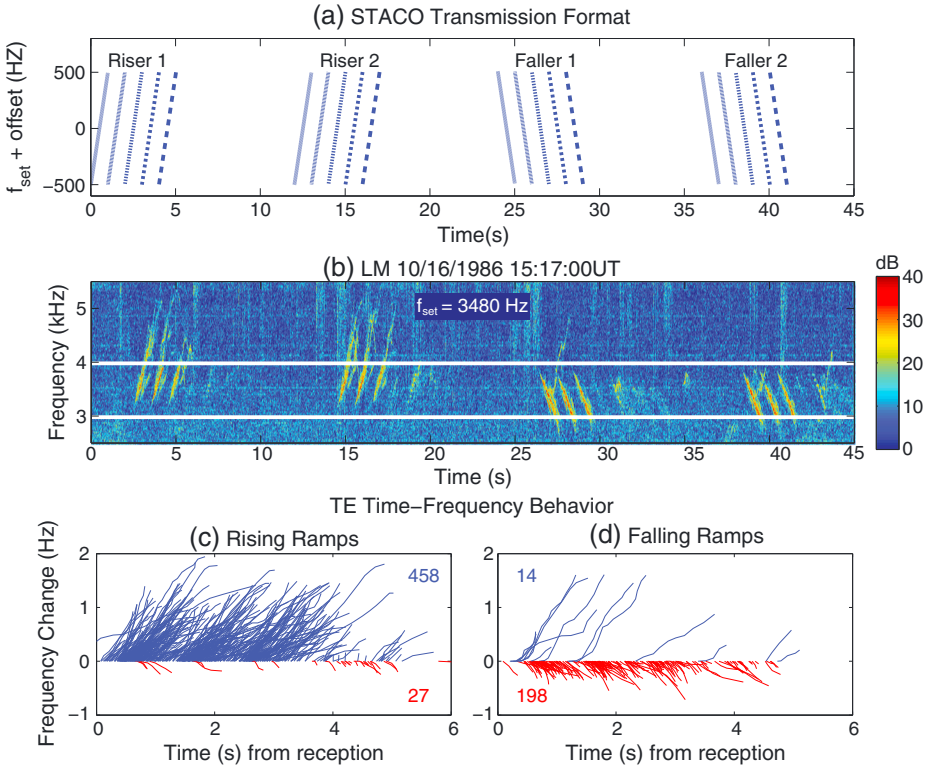

Figure 2. Spectrograms of (a) the transmitted STACO format, and (b) an example of the received signal including triggered emissions on various elements. All collected STACO triggered emissions are overlaid on the same plot to show the frequency and time profile of risers (blue) and fallers (red) triggered by (c) rising ramps and (d) falling ramps. The vertical axis describes the triggered emission's frequency change relative to its initial triggering frequency, and the horizontal axis describes the triggered emission's initiation time relative to the time at which the transmitted signal was received. For clarity in displaying the overlay plots, hooks are not included as they would overlap with and obscure the risers and fallers, and the color-coded numbers in Figures 2d–2f describe the number of plotted risers (blue) and fallers (red) for each triggering element.

from our set of 62 complete STACO transmissions, overlay plots in Figures 2c and 2d plot the aggregate time-frequency profile of all risers (blue) and fallers (red) separated by the triggering element. For clarity, the hooks are not shown due to their overlap with other triggered emissions. The vertical axis describes the frequency change of the triggered emissions relative to their initial initiation frequency, while the horizontal axis describes when the triggered emissions began relative to the reception of a frequency ramp in the STACO transmission. These overlay plots again highlight the significant role of the triggering transmission element in determining the resulting type of triggered emission, where rising ramps tend to generate rising triggered emissions and falling ramps generate falling triggered emissions. It can also be seen that risers extend to higher frequencies and endure for longer durations than fallers. As before, the triggered emissions are again labeled as risers, fallers, or hooks and are categorized in the STACO half of Table 1 by the number and percentage of triggered emissions triggered by each transmission element (rising ramps and falling ramps).

4. Statistical Characterization of Triggered Emissions

As triggered emissions can take on complex forms and can overlap significantly in time and frequency with one another, we were unable to use an automated approach to detect triggered emissions. Instead, we visually inspected a high-resolution spectrogram of each transmission and manually identified the triggered emissions. The initiation time of each triggered emission and the specified transmission element times in the transmission format were used to identify which transmission element was the triggering element. We selected a number of features to quantify triggered emission behavior and primarily analyzed the net frequency change (frequency change) and the initial frequency sweep rate (sweep rate). The frequency change

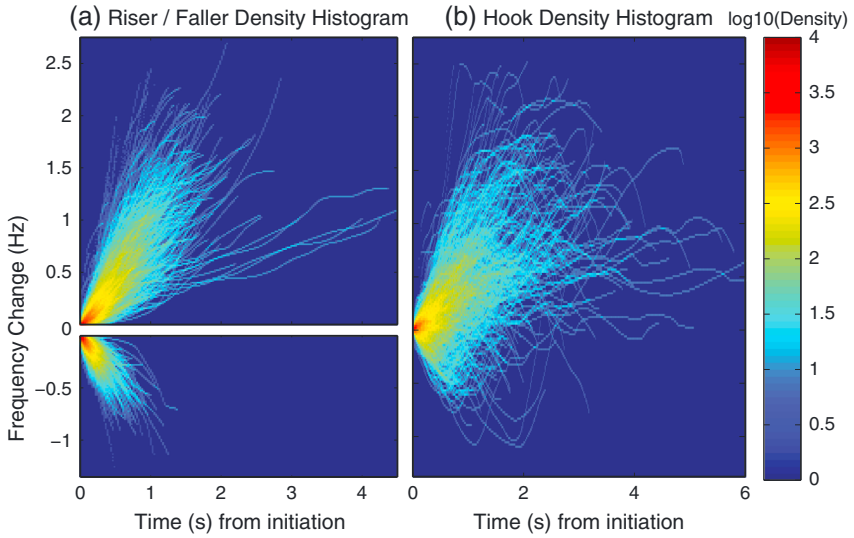

Figure 3. A two-dimensional histogram showing the density in occurrence of triggered emissions from the MDIAG format with a given time and frequency change from the triggering initiation time and frequency for (a) risers (top) and fallers (bottom), and (c) hooks. The color axis describes the number of triggered emissions in log scale.

is computed as the ending frequency minus the starting frequency. The initial sweep rate is calculated as the slope between the first two manually selected time-frequency points of the triggered emission and characterizes the instantaneous frequency sweep rate of the triggered emission at the moment of initiation. This is based on the assumption that the initial sweep rate most closely describes the initiation process and that the later behavior is driven by its own, independent interactions with the energetic electrons. Other parameters that we consider include the initial frequency at which the triggered emission began, the operator-selected f_{set} transmission frequency, the frequency at which the triggered emission ended, and the maximum frequency that the triggered emission reached.

An overview of aggregate triggered emission behavior is shown in Figure 3. Here we divide the plots of triggered emissions from the MDIAG format into the standard classes of risers, fallers, and hooks. Each 2-D histogram shows the occurrence of triggered emissions and their change in time and frequency relative to their triggering initiation time and frequency. The stacked histogram of risers and fallers in Figure 3a illustrates their differing extent of frequency change and time duration, and a comparison with the hooks in Figure 3b on their right demonstrate how hooks could be considered as combinations of risers and fallers. The color reflects the density of triggered emissions in a given time and frequency bin and the high-density regions indicate a narrow cone of behavior for risers and fallers that can be used to define the prototypical riser and faller. This high-density cone also indicates that many triggered emissions last only a short duration, < 0.5 s, and undergo only small amounts of frequency change, ~200 Hz, and that the fallers fall at a slightly higher sweep rate than risers rise. Overall, the risers last for a longer duration and extend to significantly higher frequencies than fallers, about twice as much in both respects. The hooks fill in the empty region between risers and fallers and also exhibit behavior similar to combinations of the risers and fallers.

We consider the statistical characteristics of triggered emission behavior, as shown in Figure 4. Figures 4a–4c show histograms of the net frequency change for triggered emissions triggered by the (a) long tone, (b) short tones, and (c) falling ramps. Figures 4d–4f show histograms of the initial sweep rate for triggered emissions from the (d) long tone, (e) short tones, and (f) falling ramps. Figures 4g–4i show scatterplots showing sweep rate versus frequency change for triggered emissions from the (g) long tone, (h) short tones, and (i) falling ramps. And Figures 4j–4l show scatterplots of frequency change versus initial frequency for triggered emissions from the (j) long tone, (k) short tones, and (l) falling ramps. All blue plot elements represent risers, while red elements represent fallers. In Figures 4g–4i, the magenta elements in quadrants II and IV represent hooks, where the initial sweep rate may not reflect the overall net frequency change. Each row is divided into the three main MDIAG format elements, long tone, short tones, and falling ramps, as the overlay plots in Figure 1 indicate a significant dependence on the triggering element. The text in the Figures 4a–4f details the number

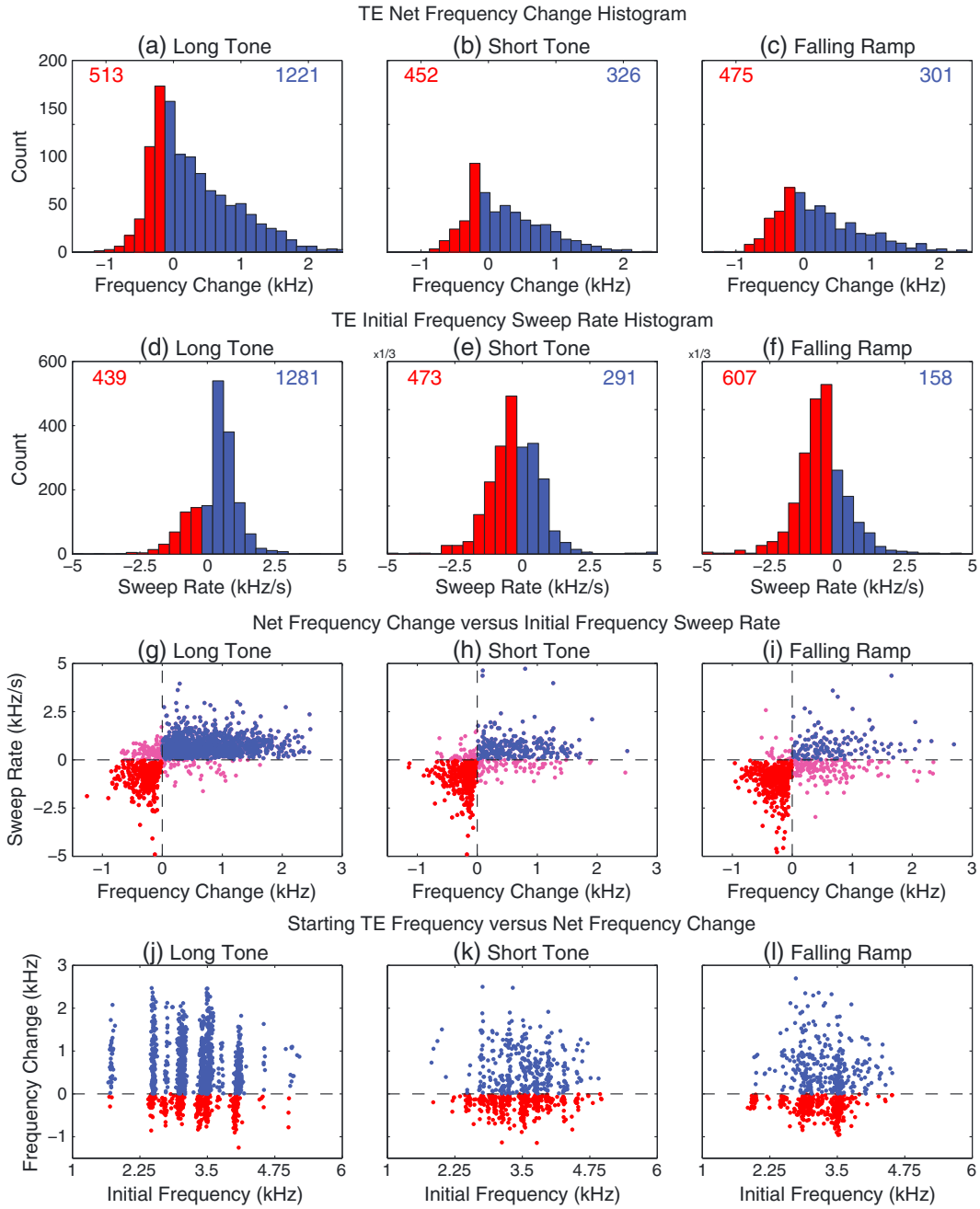

Figure 4. Analysis plots summarizing statistical observations and correlations of the time-frequency behavior of triggered emissions (TEs) excited from MDIAG transmissions. Histograms of net frequency change and initial frequency sweep rates of the triggered emissions are broken down by the triggering element type of (a, d) long tone, (b, e) short tones, and (c, f) falling ramps in the left, middle, and right columns, respectively. Blue bars illustrate net risers, while red bars illustrate net fallers. (Net frequency change includes all triggering emission types that end with positive or negative frequency change, and net sweep rate includes all triggering types that begin with positive or negative sweep rates.) The numbers in each subplot describe the number of net risers (blue) and net fallers (red) observed. The scatterplots show the frequency sweep rate as a function of the net frequency change for the (g) long tone, (h) short tones, and (i) falling ramps. The dashed black lines show the zero sweep rate and zero frequency change boundaries with risers in blue, fallers in red, and hooks in magenta. Similarly, the scatterplots show the net frequency change as a function of the initial triggered emission frequency for triggered emissions from the long tone in Figure 4g, short tones in Figure 4h, and falling ramps in Figure 4. And the dashed black line shows the zero frequency change boundary.

of net risers (blue) and net fallers (red) observed; these numbers cover all triggered emissions with a net positive or negative frequency change.

In general, from Figures 4a to 4c, the net frequency extent ranges from −1 kHz to 2.5 kHz, with risers undergoing a larger change in frequency than fallers, a median change of 558 Hz compared with −198 Hz for fallers. More specifically, the long tone exhibits significantly more triggered emissions and a preference for exciting more risers than fallers. The set of five short tones and the falling ramps preferentially excite fallers, and the short tone triggered emissions tend to undergo smaller changes in frequency. From Figures 4d to 4f, we see the preference at initiation for the long tone to excite more risers and for the short tone and the falling ramps to excite more fallers and that for all triggered emissions the initial frequency sweep rate ranges from −5 kHz/s to 5 kHz/s, although 97.8% of the cases are between −2.5 kHz/s and 2.5 kHz/s. We can also compare the sweep rate versus the net frequency change as shown in Figures 4g–4i. As before, the long tone appears to trigger more risers and the short tones and falling ramps trigger more fallers. Furthermore, this presentation of a scatterplot allows the examination of hooks as well, in magenta. The long tone generates more rising hooks, while the short tones and falling ramps produce more negative hooks. Another interesting result is that risers and fallers appear to exhibit different distributions, with fallers (red) in the lower left quadrant demonstrating a much smaller range in frequency change and sweep rate than the risers (blue) in the upper right quadrant.

While we compared a number of frequency parameters, between the initial frequency, the ending frequency, the maximum frequency, the transmission frequency, the frequency change, and the frequency sweep rate, we show just one comparison in Figures 4j–4l between the frequency change and the initial frequency of triggered emissions. There appears to be a weak trend in Figure 4j where the extent in frequency change decreases as the initial frequency increases, but there is no definitive correlation due to fewer cases at the high and low initial frequencies. And to avoid any confusion, the apparent structure of the scatterplot in Figure 4j is due to the limited discrete transmission frequencies used, while the lack of such structure in Figures 4k and 4l is due to the multiple offsets in frequency from f_{set} with the short tones and falling ramps in a transmission. Comparison of the frequency change with the f_{set} transmission frequency, the ending triggered emission frequency, and the triggered emission maximum frequency also reveals no correlation. Similarly, the frequency change does not depend on the value of the *Kp* index.

In addition to considering the time-frequency behavior of individual triggered emissions, we are also interested in understanding the parameters that determine the total number of triggered emissions excited by a given transmission. We checked for a dependence of the total number of triggered emissions for an MDIAG transmission on the *Kp* at transmission in Figure 5b and also included a plot of the general *Kp* conditions under which detection occurs in Figure 5a. Figure 5a illustrates the breakdown of the *Kp* index at transmission into five quantiles and the percent of transmissions received for each quantile. We note here that transmissions are usually detected more often when *Kp* is low, which is in good agreement with the quieting conditions of *Kp* for reception of Siple signals noted in *Li et al.* [2014]. The conditions of lower *Kp* are likely required in order for the formation of ducts for the propagation of ELF/VLF waves. Taking the received transmissions, we can then consider the number of triggered emissions based on the Kp conditions. Figure 5b breaks down transmissions by low (0–2), middle (3–12), and high (13+) number of triggered emissions, and the *Kp* at transmission is again divided into five quantiles. The number separations were selected by looking at a histogram of the occurrence of given counts of triggered emissions. While there does not appear to be any strong correlation between the low and middle cases of triggered emissions with *Kp*, the high number cases have a weak trend, suggesting that more disturbed geomagnetic conditions, as reflected by higher *Kp*, may result in a higher number of triggered emissions for a transmission.

Another parameter which may be important in determining the number of triggered emissions is the total amplification of the injected signal. The total growth can be measured by finding the narrowband signal amplitude of an injected transmission as in Figure 5c and subtracting the noise floor from the saturation threshold [*Li et al.*, 2014]. We measure the total growth of the long tone element from our 444 MDIAG transmissions and compare the total growth with the number of triggered emissions excited by the long tone as shown in Figure 5d. We observe that there is a weak linear correlation between the number of triggered emissions and the total growth with $\rho = 0.56$ with a p value < 0.01. The correlation is less pronounced when only considering the total number of risers or fallers, and the total number of triggered emissions is taken to be more representative of the overall triggering activity for a given transmission.

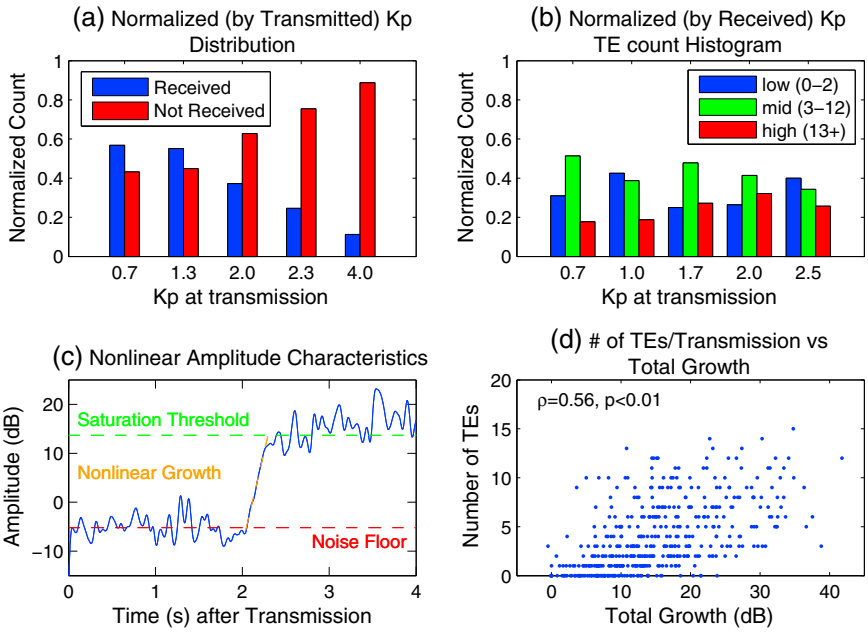

Figure 5. Five quantile *Kp* binned histograms of (a) receptions normalized by total transmissions with receptions in blue and nondetections in red and (b) of cases with low (0–2) in blue, middle (3–12) in green, and high (13+) in red number of triggered emissions. (c) An explanation plot of the amplitude characteristics of the nonlinear growth phase of the injected signal provides context for the plot of (d) the number of triggered emissions excited by the long tone in a MDIAG transmission as a function of the total growth (saturation − noise) of the transmission. The total growth and the number of triggered emissions are linearly correlated with $\rho = 0.56$ with a p value < 0.01.

Furthermore, the observed frequency-time dispersion of the falling frequency ramps in the MDIAG format can be utilized to estimate the L shell and the cold electron density at the equator, N_{eq}, of the path of propagation [*Golkowski*, 2009, section 3.2]. For the observations where the ramp element was present, we calculate the cold plasma parameters associated with the transmission. The L shell ranges from ~3.5 to ~6.5, and the N_{eq} values range from ~1 el cm^{-3} to ~600 el cm^{-3}. No correlation is observed between the number of triggered emissions or the initial triggered emission frequency sweep rate and the L shell of N_{eq}. This differs from the work by *Nunn et al.* [2005], which found a strong dependence of the emission sweep rate on the cold electron density at the equator. Hot plasma parameters from in situ satellite measurements are not available for these intervals.

By applying a similar analytic method to triggered emissions from STACO transmissions of ±1 kHz/s ramps, we extend our analysis to also compare the effects of an injected rising versus falling frequency ramp (although the amplitude analysis and the L shell and N_{eq} comparisons are only applied to the MDIAG data). As the staircase tones approximate ramps quite closely, we can consider the vast majority of triggered emissions as having been triggered from the ramps, with the 100 ms tone approximation as the only exception. The results in Figure 6 show two histograms quantifying the (a and b) net frequency change and (c and d) initial frequency sweep rate behavior of triggered emissions excited from rising (left column) and falling (right column) ramps, as well as two scatterplots (e and f) showing sweep rate versus frequency change. Again, all blue plot elements represent risers, while red elements represent fallers, and as before, the magenta elements in Figures 4g–4i represent hooks. The plots in Figures 6a, 6c, and 6e correspond with triggered emissions from rising ramps, while the plots in Figures 6b, 6d, and 6f correspond with triggered emissions from falling ramps. The inset text in the subfigures describes the total number of risers (blue) and fallers (red) observed.

While the results from analyzing STACO transmissions, as shown in Figures 6a–6d, demonstrate similar ranges in net frequency change and initial frequency sweep rates as the MDIAG triggered emissions, the triggering effect of different transmission elements is significantly more pronounced. Rising ramps (Figures 6a and 6c) show a clear and strong preference for risers, with a median frequency increase of 391 Hz and a median initial sweep rate of 1.03 kHz/s, while the falling ramps (Figures 6b and 6d) show the opposite preference for fallers, with a median frequency change of −166 Hz and a median sweep rate of −0.73 kHz/s. This preferential

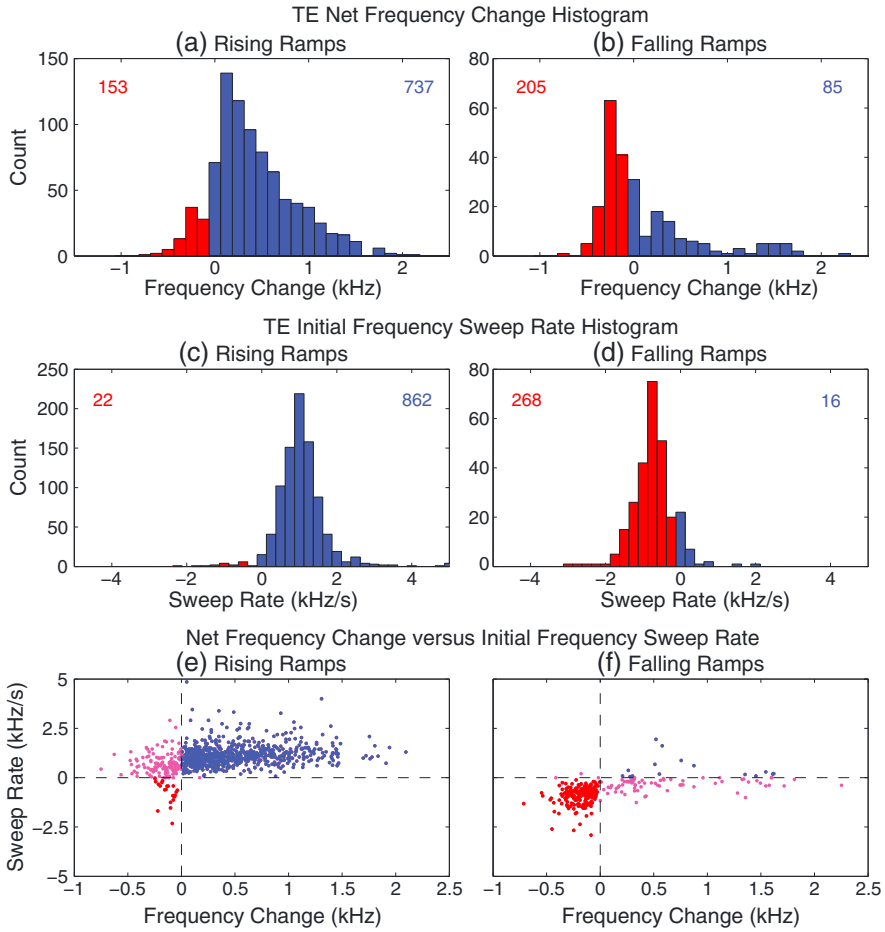

Figure 6. Analysis plots summarizing statistical observations and correlations of the time-frequency behavior of triggered emissions (TEs) excited from STACO transmissions. Histograms of net frequency change and initial frequency sweep rates of the triggered emissions are broken down by (a, c) rising and (b, d) falling ramps. Blue bars illustrate net risers, while red bars illustrate net fallers. (Net frequency change includes all triggering emission types that end with positive or negative frequency change, and net sweep rate includes all triggering types that begin with positive or negative sweep rates.) The numbers in each subplot describe the number of net risers (blue) and net fallers (red) observed. The scatterplots show the frequency sweep rate as a function of the net frequency change for (e) rising and (f) falling ramps. The dashed black lines show the zero sweep rate and zero frequency change boundaries with fallers in red, risers in blue, and hooks in magenta.

triggering extends to the hooks generated, as shown in Figures 6e and 6f, where rising ramps generate almost exclusively positive hooks and falling ramps negative hooks. Although the STACO and MDIAG falling ramps are both −1 kHz/s ramps, any difference in behavior may be attributed to the larger number of ramps in the STACO format and to human error in labeling the triggering element for the MDIAG format.

For reference, we have included tabulated results describing the median net frequency change and initial frequency sweep rate behavior of triggered emissions from MDIAG and STACO transmissions in 1986. Table 2 describes both the median frequency change for net risers and fallers and the median frequency sweep rate for initial risers and fallers, as triggered by long tones, short tones, falling ramps, and rising ramps. The breakdown supports again the analysis characterizing risers as undergoing more frequency change than fallers as well as the observation that the transmission type or element plays a significant role in determining the initial triggering response such as in the initial frequency sweep rate. Several cells are left blank, due to an insufficient number of triggered emissions for analysis.

5. Discussion and Model Validation

These statistical characterizations of triggered emission behavior can be used to direct theoretical exploration and to constrain numerical simulations of triggered emissions. From Figures 4a to 4f and Figures 6a to 6d, we

Table 2. Table of MDIAG and STACO Triggered Emission Statistics in 1986, Illustrating the Median Frequency Change for Net Risers and Fallers and the Median Frequency Sweep Rate for Initial Risers and Fallers Triggered by Each Element of the MDIAG and STACO Transmission Formats[a]

	Net Riser ΔFrequency	Net Faller ΔFrequency	Initial Riser Sweep Rate	Initial Faller Sweep Rate
		MDIAG		
All	558 Hz	−198 Hz	581 Hz/s	−735 Hz/s
Long tone	601 Hz	−214 Hz	602 Hz/s	−726 Hz/s
Short tones	536 Hz	−155 Hz	520 Hz/s	−681 Hz/s
Falling ramps	536 Hz	−252 Hz	571 Hz/s	−817 Hz/s
Doublet	— —	— —	— —	— —
		STACO		
All	397 Hz	−155 Hz	1017 Hz/s	−726 Hz/s
Rising ramps	391 Hz	−145 Hz	1025 Hz/s	— —
Falling ramps	477 Hz	−166 Hz	— —	−726 Hz/s

[a]Net riser or faller indicates a triggered emission with overall positive or negative frequency change, and initial riser or faller includes a triggered emission with initial positive or negative sweep rate.

find that overall, triggered emissions have a net frequency change between −1 kHz and 2.5 kHz and initiate with an initial sweep rate ranging between −2.5 kHz/s and 2.5 kHz/s. We also observe that risers appear to undergo a wider range in net frequency change than fallers, as noted by the spread in Figures 4g–4i and to a lesser extent in Figures 6e and 6f and as summarized by the median frequency change values of 397 Hz to 601 Hz for the risers and of −145 Hz to −252 Hz for the fallers in Table 2. This typical triggered emission behavior is also illustrated in an alternate form by Figure 3a, where the cone of higher occurrence illustrates the difference in frequency and time extent between the risers and fallers. This difference in behavior between risers and fallers hints at potential differences in conditions suitable for generation and sustained evolution of triggered emissions based on their initial type and may relate to the observed preferential amplification of rising frequency ramps in *Li et al.* [2015]. While the precise physical mechanism is not yet known, one possible explanation is suggested by *Li et al.* [2015], which found that injected rising ramps are preferentially amplified due to favorable linear growth rate conditions that allow for an earlier initiation of nonlinear amplification. Similarly, risers may be preferentially amplified over fallers as the experimental conditions may allow for a larger range of frequencies to support continued amplification of risers. The linear growth rate curve as a function of frequency also decreases more rapidly as the frequency decreases but more gradually as the frequency increases. Nonlinear effects are also likely important, but some basic differences in behavior are already evident from the linear growth rate profile. There are some suggestions that the range of frequency change depends slightly on the initial frequency of the triggered emission as observed by the range of frequency changes observed in Figure 4j, but there is an insufficient number of receptions at higher f_{set} frequencies. Figure 3b also suggests that the overall frequency-time behavior of hooks can be considered as a combination of risers and fallers.

Another important result is that format of the original triggering element directly impacts the resulting triggered emissions. Here we clearly show that long tones (Figures 4a and 4d), short tones (Figures 4b and 4e), falling ramps (Figures 4c and 4f and Figures 6a and 6c), and rising ramps (Figures 6b and 6d) each exhibit a particular preference in the initial behavior of the triggered emission. Specifically, the differences in triggering behavior can be attributed to the two primary factors of duration and sweep rate of the triggering signal. We note that the difference in duration between the long tone and the short tones and the difference in the rising versus falling ramps result in the generation of quite different triggered emissions, where the long tone and rising ramps favor risers (45% and 51%) and positive hooks (29% and 45%), while the short tones and falling ramps favor fallers (49%, 56%, and 68%) and negative hooks (13%, 23%, and 25%). These differences in triggered emission types are illustrated by the traces of the different triggered emissions in Figures 1d–1f and Figures 2c and 2d and broken down by percentage in Table 1. Consequently, a theory of triggered emissions should address the dependence on the form of the triggering signal, and numerical simulations of triggered emissions should reproduce a range of triggered emissions just by varying the signal duration and sweep rate. Despite this dependence on the form of the triggering signal, the triggered emissions can also become quite

free-running at a later time point. This can be noted by the large number of hooks that are triggered which undergo varied frequency sweep rate changes over time, as shown in the aggregate by the hooks in Figure 3b.

Theoretical treatment or numerical simulations of the triggered emission process should also reproduce wave amplification, as triggered emissions typically occur after the transmitted signal reaches saturation and ceases amplification, or when the signal terminates [*Stiles and Helliwell*, 1977]. However, the dependence of triggering behavior on signal amplitude leads to some difficulty in determining the exact theoretical contribution of the duration and sweep rate of the triggering signal on the triggered emission behavior, as the same two features also play a role in determining the amplification of the triggering signal [*Helliwell and Katsufrakis*, 1974; *Li et al.*, 2015]. Future examination of the two ramps of differing power in the MDIAG format may provide some insight into the effect of amplitude versus sweep rate on the resulting triggered emissions. We also note that the doublets produce very few triggered emissions, supporting the observed suppression effect from certain wave-wave interactions [*Helliwell*, 1983]. The weak trend of more triggered emissions occurring when *Kp* at transmission is higher, from Figure 5b, implies that more disturbed conditions reflect distributions with higher energy, allowing for more triggering. Similarly, the moderate correlation between the number of generated triggered emissions and the total growth of the injected signals in Figure 5d implies that the energy available for nonlinear amplification relates to the energy available for the generation and amplification of triggered emissions.

The STACO triggered emission behavior, in Figures 6a–6d, also revisits the question regarding when the triggering signal ends and the triggered emission begins. *Stiles and Helliwell* [1975] first raised this question in observing that triggered emissions begin at the same frequency as the triggering signal and that the two signals could not be separated. *Stiles and Helliwell* [1975] then, somewhat arbitrarily, defined only the unamplified signal as the injected or triggering signal. We revisit this question as the triggered emissions from the STACO ramps not only begin at the same frequency as the triggering signal but also initiate at the same frequency sweep rate. For the rising ramps rising at 1 kHz/s, the triggered risers begin with a median initial frequency sweep rate of 1.03 kHz/s. And for the falling ramps at −1 kHz/s, the sweep rates of the triggered fallers are still quite close at −0.73 kHz/s. Tones may exhibit similar behavior with triggered emissions initiating with a 0 kHz/s sweep rate but are difficult to detect as such behavior would simply lengthen the tone. This behavior of the triggered emission as an extension or reradiation of the injected signal has some implication on understanding the triggering process and may tie in with the wave amplification process. As we note in simulations of wave amplification [*Harid et al.*, 2014], the amplification process can result in a lengthening of the injected pulse, which may actually correspond with the generation of a triggered emission.

We briefly consider how our statistical observations might update the observations and features described by *Stiles and Helliwell* [1975]. *Stiles and Helliwell* [1975] provided a first statistical description of triggered emission behavior by analyzing the time evolution of spectral profiles of triggered emissions. In his study, he examined triggered emissions observed from several days in 1963 of constant frequency tones transmitted by the NAA and the Forestport, New York, Omega transmitters and received at Eights Station, Antarctica, as well as constant frequency tones transmitted from Siple Station, Antarctica, and received at Roberval, Quebec, Canada. Of the conclusions presented by *Stiles and Helliwell* [1975], we address the points regarding the time-frequency behavior (1–5 and 7). We agree that (1) triggered emissions "begin at the frequency of the transmitted signal" and for the most part (3 and 4) that the "initial low-amplitude portions of the [triggered emissions] stimulated by Siple, … , are also fairly repeatable" and are generally well behaved. In part, we also agree that (2) some triggered emissions, "regardless of their final slope, initially rise upon leaving the triggering frequency," but have noted several cases which do not conform to this behavior. This statement may also be true more so for a limited subsection of low-powered tones in his original study, as falling frequency ramps quite commonly trigger pure fallers. We cannot comment for certain on (7) that "the generation process [of triggered emissions] is relatively independent of transmitter frequency and power," as we only examine data from Siple Station, which were also significantly more powerful in 1986 than in 1963. However, we believe that our observations of triggered emissions appear more varied than those observed in *Stiles and Helliwell* [1975]. Finally, we disagree strongly with (5) that the triggered emissions from Siple "rarely drift more than 100 Hz above the triggering frequency before the triggering signal has terminated." In fact, we find that triggered emissions from Siple can drift far more than 100 Hz from the triggering frequency before the injected signal terminates and can undergo very significant overall changes in frequency.

Similarly, we can consider how our observations can update the features of triggered emissions covered in the review papers presented by *Matsumoto* [1979] and *Omura et al.* [1991]. Of the features concerning the time-frequency behavior in *Omura et al.* [1991] (1 and 2, and 4), we agree that (1) triggered "emissions have a narrow bandwidth" and that (4) triggered emissions undergo considerable "total frequency change" and can exhibit "complex emission forms." However, we disagree with (2) that triggered emissions are "long enduring" with a duration "many times that of the triggering pulse." Instead, we find that although there are emissions of long duration, many triggered emissions endure for only a short time, commonly lasting less than 0.5 s and for a shorter duration than the triggering pulse. Overall, our observations illustrate that triggered emissions are even more complex and varied in behavior than earlier observations indicated, with greater observed ranges in the extent of frequency change and of triggered emission duration.

These statistical bounds and features can be used to validate numerical simulations of triggered emissions. Next, we compare our statistical observations with three types of models used to simulate triggered emissions. Of the many approaches, for instance, described in Table 1 of *Omura et al.* [1991], we consider simulation results from two Vlasov type codes by *Nunn et al.* [2003] and *Harid et al.* [2014], a PIC approach by *Hikishima and Omura* [2012], and a phenomenological theory by *Helliwell* [1967]. These approaches are fairly successful in reproducing aspects of triggered emissions. *Nunn et al.* [2003] produces a canonical riser and faller and a reasonable hook. *Harid et al.* [2014] models wave amplification but shows how triggering can occur at the termination of an injected signal. *Hikishima and Omura* [2012] also generates risers, and *Helliwell* [1967] demonstrates how to reproduce the spectral form of a given triggered emission. The primary limitation is that each approach only reproduces limited features or a limited type of triggered emissions. The VHS code by *Nunn et al.* [2003] reproduces all three types of triggered emissions, but the bandwidth constraints of the code do not accurately reproduce the observed triggered emission bandwidths and require additional constraints in order to reproduce saturation effects which may play a role in determining triggered emission occurrence. *Harid et al.* [2014] does not require bandwidth filtering constraints but only generates triggered emissions with quite limited frequency change. The PIC approach of *Hikishima and Omura* [2012] requires few assumptions and addresses a number of other physical characteristics but is limited to producing risers with sweep rates on the order of 1 kHz/s. These results of the numerical simulations contrast directly with our statistics, which show triggered emissions of all types being generated by the same injected signal in the same duration and with frequency changes on the order of several kilohertz. Even when the sweep rates are reasonable, such as a riser sweep rate of 2 kHz/s and a faller sweep rate of −2 kHz/s, the frequency change extent may push the limits of our observations, where the riser undergoes a frequency change of 1.5 kHz and a faller of −2 kHz [*Nunn et al.*, 2003]. And the spectral forms of the modeled triggered emissions [*Nunn et al.*, 2003; *Hikishima and Omura*, 2012] are often also of a very simple time-frequency form unlike the complexities observed in the data. On the other hand, the phenomenological theory presented by *Helliwell* [1967] can reproduce a wide range of observed triggered emissions but requires a large number of free parameters, making parametric simulation rather complicated. To aid in the development of reasonable models, we suggest a number of features that should be reproduced. Most importantly, the model should be able to generate a wide range of frequency sweep rates and reach a wide range of frequency changes, in accordance with observations of triggered emissions. Furthermore, different types of injected elements should trigger proportionally different types of triggered emissions.

6. Conclusions

The understanding and modeling of the generation of ELF/VLF triggered emissions continue to pose a challenge for further scientific work, and advances in theoretical explanations and in numerical simulations can aid in the understanding of broader aspects of wave-particle interactions in the magnetosphere. While different models can successfully model aspects of triggered emissions, no single simulation approach captures the full range of triggered emission behavior as observed in the data. To aid in theoretical and modeling efforts to reproduce the full behavior of triggered emissions, we present an improved data set of 4650 triggered emissions generated from two different formats transmitted by the Siple Experiment over nine months in 1986. Using our database of triggered emissions, we find a number of results that are listed below:

1. Triggered emissions can exhibit a wide range of frequency sweep rates, between −2.5 kHz/s and +2.5 kHz/s, and undergo significant frequency change between −1 kHz and 2.5 kHz. The emissions can last up to several seconds, usually no more than 4 s but can also be quite short, < 0.5 s.

2. Triggering behavior at the initiation of triggering appears to depend on the transmitted element but can become quite free running at a later time point.
3. The orientation of transmitted frequency ramps is very important in determining the initial triggered emission profile. Rising ramps generate initial risers 97.5% of the time, while falling ramps trigger initial fallers 94.4% of the time. And the resulting triggered emission sweep rates, 1.03 kHz/s for risers and −0.73 kHz/s for fallers, are close to the transmitted ramp's sweep rate of ±1 kHz/s.
4. The duration of constant frequency tones plays a role in determining the initial triggered emission profile. Long tones (2 s) generate initial risers 74.5% of the time, while short tones (200 ms) trigger initial fallers 61.9% of the time.
5. Risers tend to undergo larger frequency change (median changes from all triggering elements between 397 Hz and 601 Hz) than fallers (median changes of −145 Hz to −252 Hz), regardless of the triggering element. And risers can endure for longer duration (<5 s) than fallers (<2 s).
6. The number of triggered emissions is linearly dependent on the total growth of the transmitted signal and may correlate with more disturbed geomagnetic conditions, as describe by the *Kp* index.

These results substantially improve the statistical understanding of triggered emission behavior. We expect that these statistical bounds will be useful in directing theoretical examination of the triggering process and in validating numerical simulations to better understand wave-particle interactions in the magnetosphere. Further work in analyzing the amplitude behavior of triggered emissions may also be useful for comparing observations and theory.

Acknowledgments
This work is supported by AFRL award FA9453-11-C-0011 to Stanford University. We are grateful to Vijay Harid and Timothy Bell for helpful discussions. Requests for the data used in the analysis can be directed to the corresponding author.

Michael Balikhin thanks the reviewers for their assistance in evaluating this paper.

References

Carpenter, D. L., K. Stone, and S. Lasch (1969), A case of artificial triggering of VLF magnetospheric noise during the drift of a whistler duct across magnetic shells, *J. Geophys. Res.*, *74*, 1848–1855, doi:10.1029/JA074i007p01848.

Gibby, A. R., U. S. Inan, and T. F. Bell (2008), Saturation effects in the VLF-triggered emission process, *J. Geophys. Res.*, *113*, A11215, doi:10.1029/2008JA013233.

Golkowski, M. (2009), Magnetospheric wave injection by modulated HF heating of the auroral electrojet, PhD dissertation, Stanford Univ., Stanford, Calif.

Harid, V., M. Golkowski, T. Bell, J. D. Li, and U. S. Inan (2014), Finite difference modeling of coherent wave amplification in the Earth's radiation belts, *Geophys. Res. Lett.*, *41*, 8193–8200, doi:10.1002/2014GL061787.

Helliwell, R. A. (1965), *Whistlers and Related Ionospheric Phenomena*, Stanford Univ. Press, Stanford, Calif.

Helliwell, R. A. (1967), A Theory of discrete VLF emissions from the magnetosphere, *J. Geophys. Res.*, *72*, 4773–4790, doi:10.1029/JZ072i019p04773.

Helliwell, R. A. (1970), The upper atmosphere as seen from Antarctica, *Bull. At. Sci.*, *26*(10), 55–61.

Helliwell, R. A. (1979), Siple Station experiments on wave-particle interactions in the magnetosphere, in *Wave Instabilities in Space Plasmas, Proceedings of a Symposium Organized Within the 19th URSI General Assembly Held in Helsinki, Finland, July 31–August 8, 1978*, edited by P. J. Palmadesso and and K. Papadopoulos, pp. 191–203, D. Reidel, Dordrecht.

Helliwell, R. A. (1983), Controlled stimulation of VLF emissions from Siple Station, Antarctica, *Radio Sci.*, *18*, 801–814, doi:10.1029/RS018i006p00801.

Helliwell, R. A. (1988a), VLF wave stimulation experiments in the magnetosphere from Siple Station, Antarctica, *Rev. Geophys.*, *26*, 551–578, doi:10.1029/RG026i003p00551.

Helliwell, R. A. (1988b), VLF wave-injection experiments from Siple Station, Antarctica, *Adv. Space Res.*, *8*, 279–289, doi:10.1016/0273-1177(88)90373-0.

Helliwell, R. A., and D. L. Carpenter (1962), Whistler-west results from the IGY-IGC-59 synoptic program, *Eos Trans. AGU*, *43*, 125.

Helliwell, R. A., and T. L. Crystal (1973), A feedback model of cyclotron interaction between whistler-mode waves and energetic electrons in the magnetosphere, *J. Geophys. Res.*, *78*, 7357–7371, doi:10.1029/JA078i031p07357.

Helliwell, R. A., and J. P. Katsufrakis (1974), VLF wave injection into the magnetosphere from Siple Station, Antarctica, *J. Geophys. Res.*, *79*(16), 2511–2518, doi:10.1029/JA079i016p02511.

Helliwell, R. A., J. P. Katsufrakis, M. L. Trimpi, and N. M. Brice (1964), Artificially stimulated very low frequency radiation from the ionosphere, *J. Geophys. Res.*, *69*, 2391–2394, doi:10.1029/JZ069i011p02391.

Helliwell, R. A., U. S. Inan, J. P. Katsufrakis, and D. L. Carpenter (1986), Beat excitation of whistler mode sidebands using the Siple VLF transmitter, *J. Geophys. Res.*, *91*, 143–153, doi:10.1029/JA091iA01p00143.

Hikishima, M., and Y. Omura (2012), Particle simulations of whistler-mode rising-tone emissions triggered by waves with different amplitudes, *J. Geophys. Res.*, *117*, A04226, doi:10.1029/2011JA017428.

Hikishima, M., Y. Omura, and D. Summers (2010), Microburst precipitation of energetic electrons associated with chorus wave generation, *Geophys. Res. Lett.*, *37*, L07103, doi:10.1029/2010GL042678.

Katoh, Y., and Y. Omura (2006), A study of generation mechanism of VLF triggered emission by self-consistent particle code, *J. Geophys. Res.*, *111*, A12207, doi:10.1029/2006JA011704.

Kimura, I. (1968), Triggering of VLF magnetospheric noise by a low-power (100 watts) transmitter, *J. Geophys. Res.*, *73*(1), 445–447, doi:10.1029/JA073i001p00445.

Lasch, S. (1969), Unique features of VLF noise triggered in the magnetosphere by Morse-code dots from NAA, *J. Geophys. Res.*, *74*, 1856–1858, doi:10.1029/JA074i007p01856.

Li, J. D., M. Spasojevic, V. Harid, M. B. Cohen, M. Golkowski, and U. S. Inan (2014), Analysis of magnetospheric ELF/VLF wave amplification from the Siple Transmitter Experiment, *J. Geophys. Res. Space Physics*, *119*, 1837–1850, doi:10.1002/2013JA019513.

Li, J. D., V. Harid, M. Spasojevic, M. Golkowski, and U. S. Inan (2015), Preferential amplification of rising versus falling frequency whistler mode signals, *Geophys. Res. Lett.*, *42*, 207–214, doi:10.1002/2014GL062359.

Matsumoto, H. (1979), Nonlinear whistler-mode interaction and triggered emissions in the magnetosphere: A review, in *Wave Instabilities in Space Plasmas*, edited by P. J. Palmadesso and and K. Papadopoulos, pp. 163–190, Springer, Netherlands.

Mielke, T. A., and R. A. Helliwell (1993), Siple Station, Antarctica, experiments on staircase frequency ramps as approximations to continuous ramps, *J. Geophys. Res.*, *98*, 4053–4061, doi:10.1029/92JA02562.

Nunn, D., A. Demekhov, V. Trakhtengerts, and M. J. Rycroft (2003), VLF emission triggering by a highly anisotropic energetic electron plasma, *Ann. Geophys.*, *21*(2), 481–492, doi:10.5194/angeo-21-481-2003.

Nunn, D., M. Rycroft, and V. Trakhtengerts (2005), A parametric study of the numerical simulations of triggered VLF emissions, *Ann. Geophys.*, *23*(12), 3655–3666, doi:10.5194/angeo-23-3655-2005.

Omura, Y., D. Nunn, H. Matsumoto, and M. J. Rycroft (1991), A review of observational, theoretical and numerical studies of VLF triggered emissions, *J. Atmos. Terr. Phys.*, *53*(5), 351–368, doi:10.1016/0021-9169(91)90031-2.

Paschal, E. W. (1988), Phase measurements of very low frequency signals from the magnetosphere, PhD dissertation, Stanford Univ., Stanford, Calif.

Sa, L. A. D. (1990), A wave-particle-wave interaction mechanism as a cause of VLF triggered emissions, *J. Geophys. Res.*, *95*, 12,277–12,286, doi:10.1029/JA095iA08p12277.

Stiles, G. S., and R. A. Helliwell (1975), Frequency-time behavior of artificially stimulated VLF emissions, *J. Geophys. Res.*, *80*, 608–618, doi:10.1029/JA080i004p00608.

Stiles, G. S., and R. A. Helliwell (1977), Stimulated growth of coherent VLF waves in the magnetosphere, *J. Geophys. Res.*, *82*, 523–530, doi:10.1029/JA082i004p00523.

Trakhtengerts, V. Y., A. G. Demekhov, Y. Hobara, and M. Hayakawa (2003), Phase-bunching effects in triggered VLF emissions: Antenna effect, *J. Geophys. Res.*, *108*(A4), 1160, doi:10.1029/2002JA009415.